LOW ENERGY–HIGH FLUX NITROGEN IMPLANTATION OF AN OXIDEDISPERSION-STRENGTHENED FeAl INTERMETALLIC ALLOY

Fernando Pedraza, Jean-Luc Grosseau-Poussard, J.F Dinhut

LOW ENERGY–HIGH FLUX NITROGEN IMPLANTATION OF AN OXIDE-DISPERSION-STRENGTHENED FeAl INTERMETALLIC ALLOY

F. Pedraza[1,2], J.L. Grosseau-Poussard[2], J.F. Dinhut[2]

(1) SIFCO Turbine Components, Carrigtwohill, Co. Cork. IRELAND.

(2)LEMMA, Université de La Rochelle. 25, rue Enrico Fermi, 17042 La Rochelle Cedex 1, FRANCE.

Abstract

The oxygen-dispersion-strengthened FeAl Grade 3 intermetallic alloy has undergone a low energy-high flux nitridation treatment. The uniform implanted layer is accompanied by a random distribution of protrusions anchored by yttria particles. Electron microscopy studies reveal the presence of thin layer of AlN embedded in a matrix of FeAl, which mainly accounts for the dramatic increase in surface microhardness. After nitridation, fragmentation of the outermost FeAl grains occurs through which countercurrent diffusion of nitrogen and aluminium seems to proceed. As a result, segregation of α-Fe is observed at the nitrided layer / substrate interface.

1.- Introduction

Boron, zirconium and yttria containing binary B2 iron aluminides processed by mechanical alloying and subsequent thermal treatment lead to an oxide dispersion strengthened (ODS) intermetallic alloy of fine grain structure [**1-5**] showing -preferably in the absence of humidity- good mechanical properties [**6-8**] and oxidation resistance [**9-12**].

In intermetallic alloys, the nitridation of titanium aluminides have received most of the attention concerning the treatment itself [**13-16**], their corrosion properties [**17**] or their high temperature behaviour [**18-21**]. However, little is known on the nitridation of FeAl intermetallic alloys. To the best of our knowledge, only the oxidation kinetics and the likely mechanisms of a nitrided ODS FeAl alloy were reported in [**22**]. In this study, the effects of nitridation on the same ODS FeAl alloy are investigated by electron microscopy techniques and the likely mechanisms of formation are proposed.

2.- Experimental Procedure

FeAl40 Grade 3 containing 15 ppm B, 0.1 wt% Zr and a 1wt% Y_2O_3 dispersion were kindly supplied by CEA/CEREM (Grenoble, France) as extruded bars at 1100º C after mechanical alloying of the components. They show a strong <110> fibre texture and about 0.5-1 μm grain size [**11,22**]. Discs of 15 mm diameter, 1 mm thick were cut from the bars and subsequently mechanically polished to a final roughness of 0,01 μm. They were then ultrasonically degreased in acetone and rinsed in 96 % ethanol. Low energy – high flux nitrogen (N_2^+, N^+) implantation was carried out with a Kaufman type ion source at 1.2 keV and a current density of about 1 mA.cm^{-2} for 1 h, corresponding to an estimated dose of about 3.5 x 10^{19} at.cm^{-2}. The temperature of the samples was carefully controlled with a thermocouple attached on the back of the samples in order that it did not exceed 400°C. Prior to the nitridation treatment, Ar^+ sputtering (1.2 keV, 0.5 mA.cm^{-2} for 15 min) was carried out on each main coupon face to remove the rigid oxide layer that precludes nitridation [**23**], which partially heated the samples. The backing pressure in the chamber upon the nitriding process was better than 10^{-2} Pa. Implantation was carried out on both principal coupon faces for the subsequent oxidation experiments, representing about 85% of the overall surface.

Characterisation of the implanted and the oxidised specimens was undertaken using contact mode atomic force microscopy (AFM) with an Autoprobe CPR (Veeco Instruments), by X-ray diffraction in a Bruker AXS D-5005 equipment in the θ-2θ configuration using the Cu $K_{\alpha 1}$ (λ = 0.15406 nm) as well as by scanning electron microscopy (SEM) coupled to energy-dispersive spectrometry (EDS) in a JEOL JSM-4510 LV. Cross sections of the implanted specimens were also prepared for transmission electron microscopy (TEM) studies in a JEOL-JEM 2010 operating at 200 kV. For such purpose, careful mechanical polishing in SiC# 4000 emery paper was performed down to a thickness of about 50 μm. Then, Ar bombardment at 3 keV was carried out in a GATAN PIPS™ (precision ion polishing system) model 691 at different angles. Vickers microhardness measurements were also performed at increasing loads to get acquainted of the effects of the implantation.

3.- Results

As shown in Figure 1 (a), the morphology of the nitrided alloy is quite uniform throughout the entire surface with some remaining porosity arising from the manufacturing process as well as ridge-like and white round protrusions, of nanometre scale. EDS analyses [Figure 1 (b)] on different large areas reveal average atomic compositions of 55% Fe-25% Al and 20% N (at%), whereas point EDS on the white round particles indicate the presence of yttrium and oxygen in variable amounts together with the nitrided matrix elements, thus presumably corresponding to the Y_2O_3 dispersion. The edges of the ridges seem to be stopped at the white round particles and do not contain any yttrium. This is confirmed by AFM imaging (Figure 2), which also allows to observe that the average surface roughness rarely exceeds 0.05 μm.

The Vickers microhardness measurements as a function of the estimated indentation depths are shown in Figure 3, where it can be observed that the surface hardness is increased by about four times with respect that of the as-polished alloy. The overall estimated nitrided depth is of about 4 μm, but the highest values are encountered within the first 1.5 μm. The nitrided layer fully develops within the substrate matrix. After a chemical etch, a distinctive white layer is observed (Figure 4) with the outer surface again showing protrusions. This layer is mainly composed of FeAl containing hexagonal AlN, as inferred by three XRD peaks (2θ = 33.2, 36.1 and 38º) at lower diffraction angles than a large and high (110) peak corresponding to the substrate matrix [**22**]. Likewise, the chemical etch allows to observe the nanometre range of the grains composing the nitrided layer.

TEM cross section inspection of the parent intermetallic alloy reveals a preferential elongation of the grains throughout the thinned area of Figure 5 (a), with an average grain size between 0.5 and 1 μm, which confirms previous metallographic studies of the same substrate [**11,22**]. Random distribution of the Y_2O_3 particles is also readily observable in the dark field mode. No segregation of boron has been found in the material but that of zirconium, typically within the FeAl grains, as that shown in Figure 5 (b). Figure 5 (c) corresponds to the selected area diffraction pattern (SADP) of a grain oriented $[\bar{1}\bar{1}1]$, showing the {110} planes as well as weaker reflections of the {211}

planes. The lattice parameter calculation gives a value of a = 0.2896 nm, which agrees well with that reported by Y.B. Pithawalla [**24**] for nanocrystalline B2 FeAl particles.

The AlN containing layer developed by implantation-diffusion in the intermetallic alloy is composed of tiny equiaxed grains at the nanometre scale [Figure 6 (a)]. The 3 nm spot size EDS analyses [Figure 6 (b)] across this layer indicate a smooth decrease of nitrogen towards the surface while maintaining a constant amount of aluminium. Iron, in turn, increases continuously towards the nitride layer/substrate interface dramatically exceeding (~ 75 at%) the actual iron content in the base material (~ 60 at%). In fact, close inspection of this interface (Figure 7) shows that an iron band segregates at the nitrided layer/substrate interface. This is confirmed by point EDS analyses and it is in course of investigation by Conversion Electron Mössbauer Spectroscopy (CEMS). Diffraction patterns of the different areas point out the different features observed in these samples such as the nanometre scale of the nitrided layer characterised by the typical rings corresponding to FeAl as well as some spots at shorter distances belonging to AlN. As summarised in Table 1, some of the distances may also correspond to α-Fe.

Table 1.- Experimental d-spacings obtained with 0.15 μm-diaphragm SADPs at the nitrided layer/substrate interface in the as-nitrided intermetallic alloy and their correspondence to the planes of the identified compounds.

Experimental d-spacing, nm	FeAl JCPDS 33-20	**α-Fe JCPDS**	AlN JCPDS 25-1133
0.252	-	-	002
0.207	110	110	-
0.160	111*	-	110
0.143	200	200	-
0.119	211	211	202

* *superstructure peak*

4.- Discussion

Low energy-high flux implantation-diffusion treatments at moderate temperatures allow to produce relatively thick nitrided layers in different substrates [**25-27**]. In typical

austenitic matrices, nitridation leads to the appearance of a metastable γ_N phase [**28-30**]. However, in aluminium-containing alloys, nitridation treatments may bring about either supersaturation of nitrogen in aluminium or the formation of AlN depending on the implanted dose [**31**] and on the thermodynamic stability of the alloying elements. In the FeAl alloy, the chemical affinity of N to Al is much greater than that to Fe (e.g., ΔH_f^o = -318.0 and –10.5 kJ.mol^{-1} for AlN and Fe_4N, respectively)[**32**] so that iron nitride formation was not expected to occur.

The samples have shown a very uniform implanted surface with some protrusions at the external surface and remaining porosity. This latter feature can be mainly explained by the manufacturing process of this material, which is powder metallurgy. However, different studies have shown that nitrogen implantation may give rise to the appearance of blisters (i.e. the above mentioned protrusions) and remaining porosity owing to gas bubbles [**33**]. According to Matthews et al. [**34**], these are created above a critical dose and may be dependent on the orientation of the slip planes relative to the surface, the amount of deformation being thus dependent on the yield stress of the host material. In this study, the elongated shape of the protrusions would be related to “softer” areas of the base material, where the Y_2O_3 pinning effect is less important, as shown in by AFM in Figure 2. A combination of such deformation as well as the formation of AlN gives rise to a four-fold increase in superficial hardness, progressively decreasing inwardly down to about 4 μm deep, with the most superficial 1.5 μm being the hardest. This feature seems to be related to the decreasing amount of nitrogen present in the nitrided layer, as revealed by the EDS analyses shown in Figure 6 (b). As a matter of fact, Sonnleitner et al. [**35**] on their glow discharge optical spectroscopy (GDOS) and TEM studies of plasma nitrided aluminium found that polycrystalline hexagonal AlN was exclusively formed if the nitrogen content fell within the range 15-25 wt% (i.e. 25-40 at% in AlN). Sanghera and Sullivan [**32**] found by X-ray photoelectron spectroscopy (XPS) that nitrogen implanted at low energy and low flux into pure aluminium did not render stoichiometric AlN because of reconstruction of surface atoms upon implantation giving rise to many vacancies, interstitials and defects due to radiation damage. From our semiquantitative analyses, only the outermost layers would contain enough nitrogen to produce the hexagonal AlN phases massively and therefore, one the average values of nitrogen decrease, a mixture of FeAl containing dispersed particles of AlN occurs closer

to the nitrided layer/substrate interface. The reason why the hardness is still very high compared to that of the parent intermetallic alloy is found in the fragmentation of the FeAl grains [Figures 6 (a) and 7] found after implantation since more grain boundaries are available to increase such hardness. This fragmentation effect of the grains has also been found after nitridation of AISI 304L stainless steels [**36**]. Besides, Serventi et al. [**31**] on the aluminium implantation with $5x10^{17}$ $N^{+}.cm^{-2}$ at 150 keV, which contained 25 at% N on average, found the presence of high pressure allotropic structures of AlN and reported that the internal stress increased caused by the precipitation owing to the difference in specific volumes of the matrix and the precipitates.

Nevertheless, one of the most interesting features is the α-Fe segregation at the nitrided layer/substrate interface. From the results presented in [**22**], the broadening of the FeAl (110) peak had already been noticed. The hypothesis suggested that the formation of AlN could lead to the appearance of α-Fe, which agrees well with this study. However, the TEM studies of this work lead us to think rather to a combined mechanism of nitrogen diffusing inwardly and aluminium outwardly during the nitridation treatment. This is likely to occur since on the one hand the Al profile is constant all across the analysed layer as well as the progressive decrease of nitrogen towards the internal interface. This countercurrent diffusion would be promoted by the creation of short-circuit diffusion paths, i.e. new grain boundaries due to the above-mentioned fragmentation of grains. Although the implantation temperature of this study never exceeded 400º C, diffusion of indium (isoelectronic with aluminium) has been found to be faster than that of iron by a factor of about two in $Fe_{66}Al_{34}$ and $Fe_{50}Al_{50}$ [**37**], which helps in corroborating the suggested mechanism.

5.- Summary

Nitridation of ODS FeAl by implantation diffusion leads to the development of a layer containing hexagonal AlN in a matrix of FeAl, of very high hardness. Deformation of the layer seems to be anchored by the presence of the hardening yttria particles present in the base alloy. After nitridation, the FeAl matrix possesses a nanometre size compared to the micrometre scale of the parent material owing to fragmentation of the grains. Under the AlN-containing FeAl layer, segregation of α-Fe is shown to occur as a result of outward diffusion of aluminium to react with inwardly diffusing nitrogen.

6.- Acknowledgements

The authors gratefully acknowledge the assistance of J.P. Rivière from the LMP of the University of Poitiers for his assistance in the nitriding experiments and C. Savall from the LEMMA of the University of La Rochelle for the AFM studies. This work has been performed under the post-doctoral stay of F. Pedraza, financed by the Regional Council of Poitou-Charentes.

7.- References

1. D.G. Morris, S. Gunther, C. Briguet, Scripta Mater. 37 (1) (1997) 71.
2. A. Fraczkiewicz, A.S. Gay, M. Biscondi, Mater. Sci. Eng. A258 (1998) 108.
3. E. Cadel, D. Lemarchand, A.S. Gay, A. Fraczkiewicz, D. Blavette, Scripta Mater. 41 (4) (1999) 421.
4. M. Yamaguchi, H. Inui. K Ito, Acta Mater. 48 (2000) 307.
5. E. Cadel, A. Fraczkiewicz, D. Blavette, Mater. Sci. Eng. A309-310 (2001) 32.
6. A. Tonneau, M. Gerland, G. Hénaff, Met. Mat. Trans. 32A (2001) 2345.
7. D.G. Morris, C. Garcia Oca, J. Chao, M.A. Muñoz-Morris, Scripta Mater. 46 (2002) 843.
8. M.A. Muñoz-Morris, G. Garcia Oca, D.G. Morris, Acta Mater. 50 (2002) 2825.
9. A. Mignone, S. Frangini, A. La Barbera, O. Tassa, Corr. Sci. 40 (8) (1998) 1331.
10. C.H. Xu, W. Gao, Y.D. He, Scripta Mater. 42 (2000) 975.
11. M.A. Montealegre, J.L. González Carrasco, M.A. Morris-Muñoz, J. Chao, D.G. Morris, Intermetallics 8 (2000) 439.
12. C. Dang Ngoc Chan, C. Huvier, J.F. Dinhut, Intermetallics 9 (2001) 817.
13. C.L. Chu, S.K. Wu, Surf. Coatings Technol. 78 (1996) 211.
14. S. Thongtem, T. Thongtem, M.J. McNallan, Surf. Interface Anal. 28 (1) (1999) 61.
15. J. Magnan, G.C. Weatherly, M.C. Cheynet, Met. Mat. Trans. 30A (1) (1999) 19.
16. B. Zhao, J. Sun, J.S. Wu, Z.X. Yuan, Scripta Mater. 46 (2002) 581.
17. C.L. Chu, S.K. Wu, Surf. Coatings Technol. 78 (1996) 219.
18. T.K. Roy, R. Balasubramaniam, A. Gosh, Met. Mat. Trans. 27A (12) (1996) 3993.
19. T.K. Roy, R. Balasubramaniam, A. Gosh, Met. Mat. Trans. 27A (12) (1996) 4003.
20. H.C. Choe, Surf. Coatings Technol. 148 (2001) 77.
21. B. Zhao, J. Wu, J. Sun, B. Tu, F. Wang, Intermetallics 9 (2001) 697.

22. C. Dang Ngoc Chan, C. Huvier, J.F. Dinhut, Surf. Coatings Technol. 165 (2003) 119.
23. Y. Ando, S. Tobe, H. Tahara, T. Yoshikawa, Vacuum 65 (2002) 403.
24. Y.B. Pithawalla, M.S. El Shall, S.C: Deevi, Intermetallics 8 (2000)1225.
25. S. Picard, J.B. Memet, R. Sabot, J.L. Grosseau-Poussard, J.P. Rivière, R. Meilland, Mater. Sci; Eng. A 303 (2001) 163.
26. D.L. Williamson, J.A. Davis, P.J. Wilbur, Surf. Coatings Technol. 103-104 (1998) 178.
27. J.P. Rivière, P. Méheust, J.A. García, R. Martínez, R. Sánchez, R. Rodríguez, Surf. Coatings Technol. 158-159 (2002) 295.
28. F. Pedraza, M. Reffass, J. Balmain, G. Bonnet, J.F. Dinhut, Mater. Sci. Eng., A 357 (2003) 355.
29. F. Pedraza, M. Reffass, G. Abrasonis, C. Savall, J.P. Rivière, J.F. Dinhut, Surf. Coat. Technol. 176 (2004) 236.
30. F. Pedraza, J.L. Grosseau-Poussard, G. Abrasonis, J.P. Rivière, J.F. Dinhut, J. Appl. Phys. 94 (12) (2003) 7509.
31. A.M. Serventi, M. Vittori Antisari, Phil. Mag. B76 (4) (1997) 549.
32. H.K. Sanghera, J.L. Sullivan, Surf. Interface Anal. 27 (1999) 678.
33. M.F. Denanot, J. Delafond, J. Grilhé, Rad. Effects 88 (1986) 145.
34. A.P. Matthews, M. Iwaki, Y. Horino, M. Satou, K. Yabe, Nucl. Inst. Meth. Phys. Res. B59/60 (1991) 671.
35. R. Sonnleitner, K. Spiradek-Hahn, F. Rossi, Surf. Coatings Technol. 156 (2002) 149.
36. J.P. Rivière, P. Méheust, J.P. Villain, C. Templier, M. Cahoreau, G.Abrasonis, L. Pranevicius, Surf. Coat. Technol. 91 (2002) 6361.
37. H. Mehrer, M. Eggersmann, A. Gude, M. Salamon, B. Sepiol, Mat. Sci. Eng. A239-240 (1997) 889.

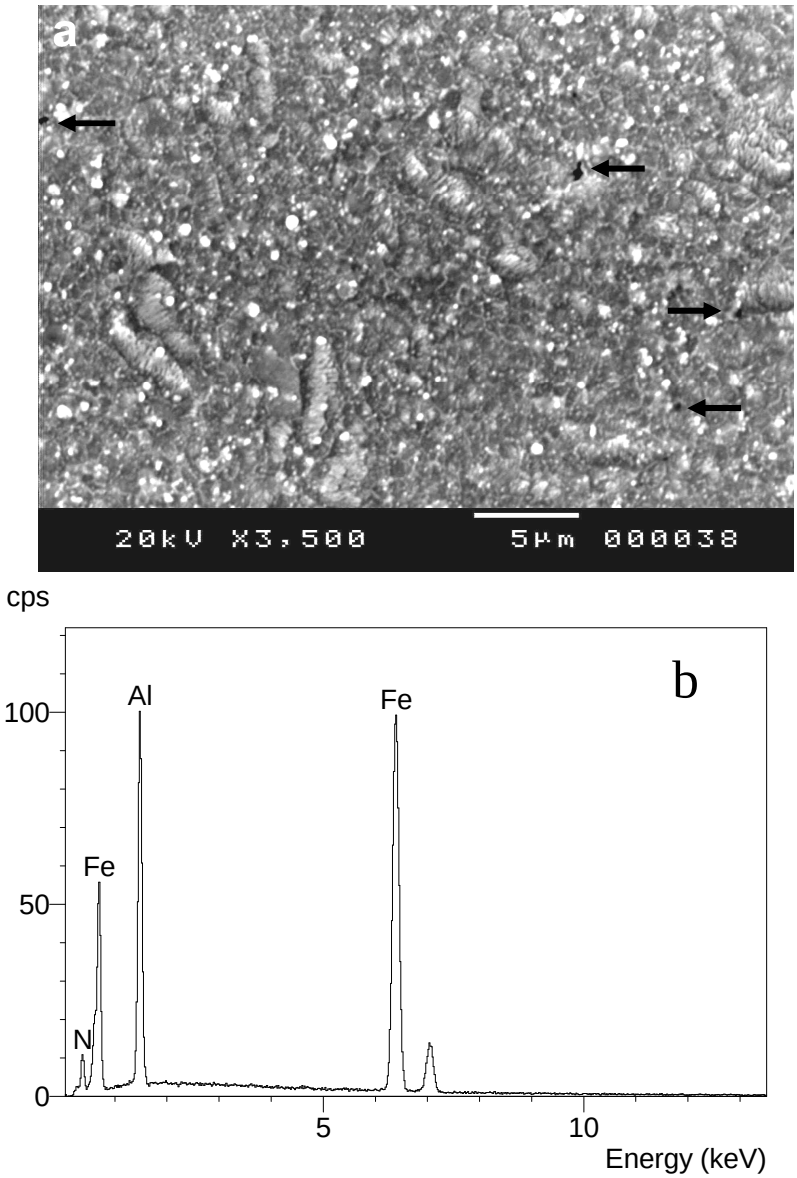

Figure 1.- SEM surface morphology of the nitrided FeAl Grade 3 showing uniformity (a) and the average EDS area analysis.

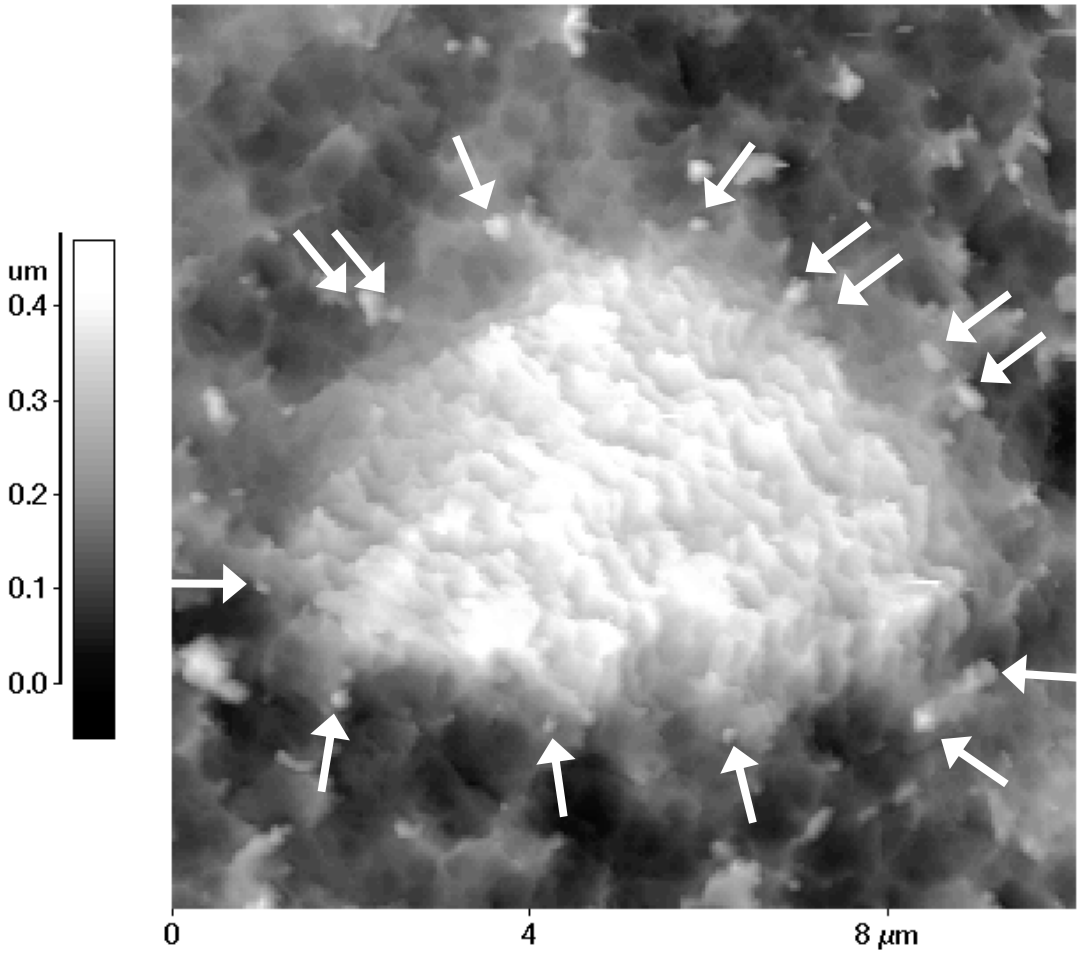

Figure 2.- AFM image of FeAl Grade 3 nitrided by implantation–diffusion showing ridges pinned by Y_2O_3 particles (view of 10 x 10 μm areas).

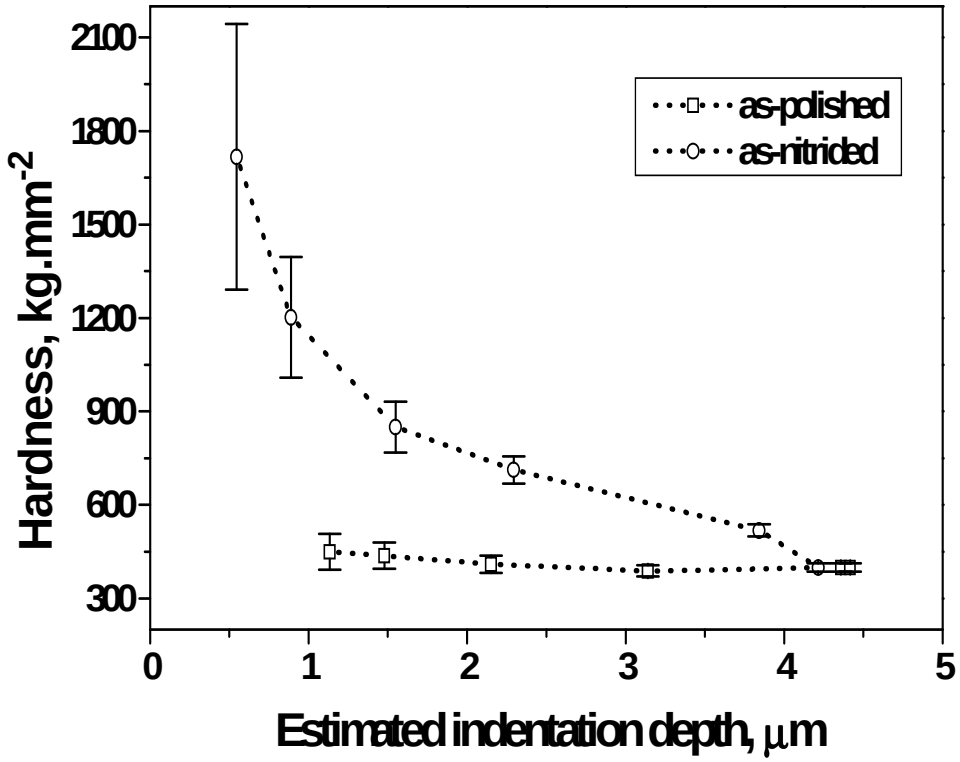

Figure 3.- Vickers microhardness values vs. applied load for the untreated and nitrided FeAl Grade 3 substrates.

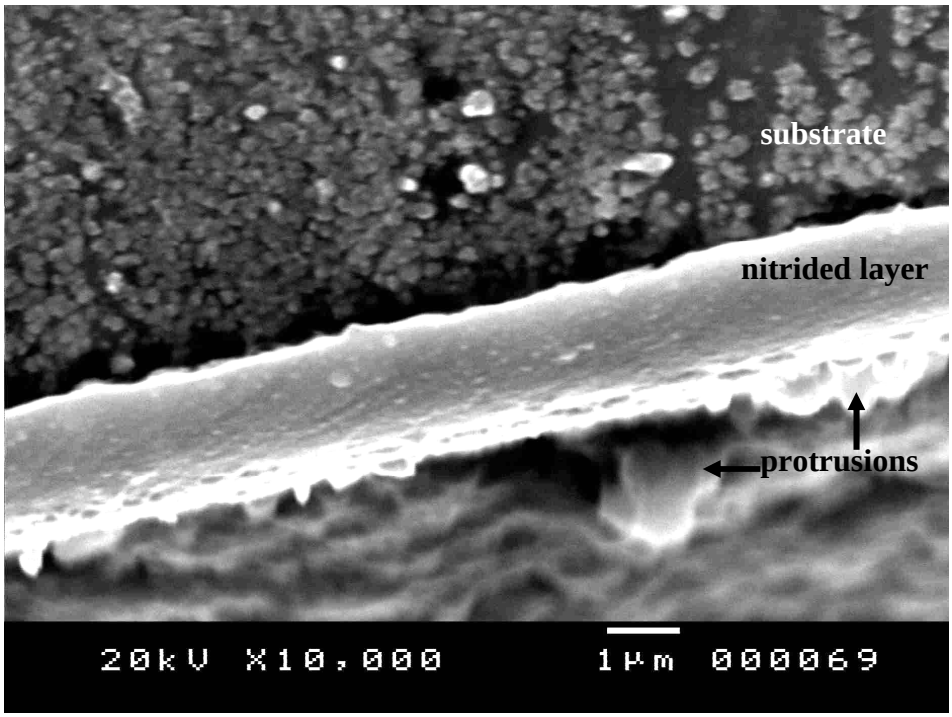

Figure 4.- SEM cross section of the nitrided FeAl Grade 3 showing thickness homogeneity of the nitrided layer as well as the appearance of protrusions at the layer/gas interface. The nanometer scale of the substrate grains is also observed.

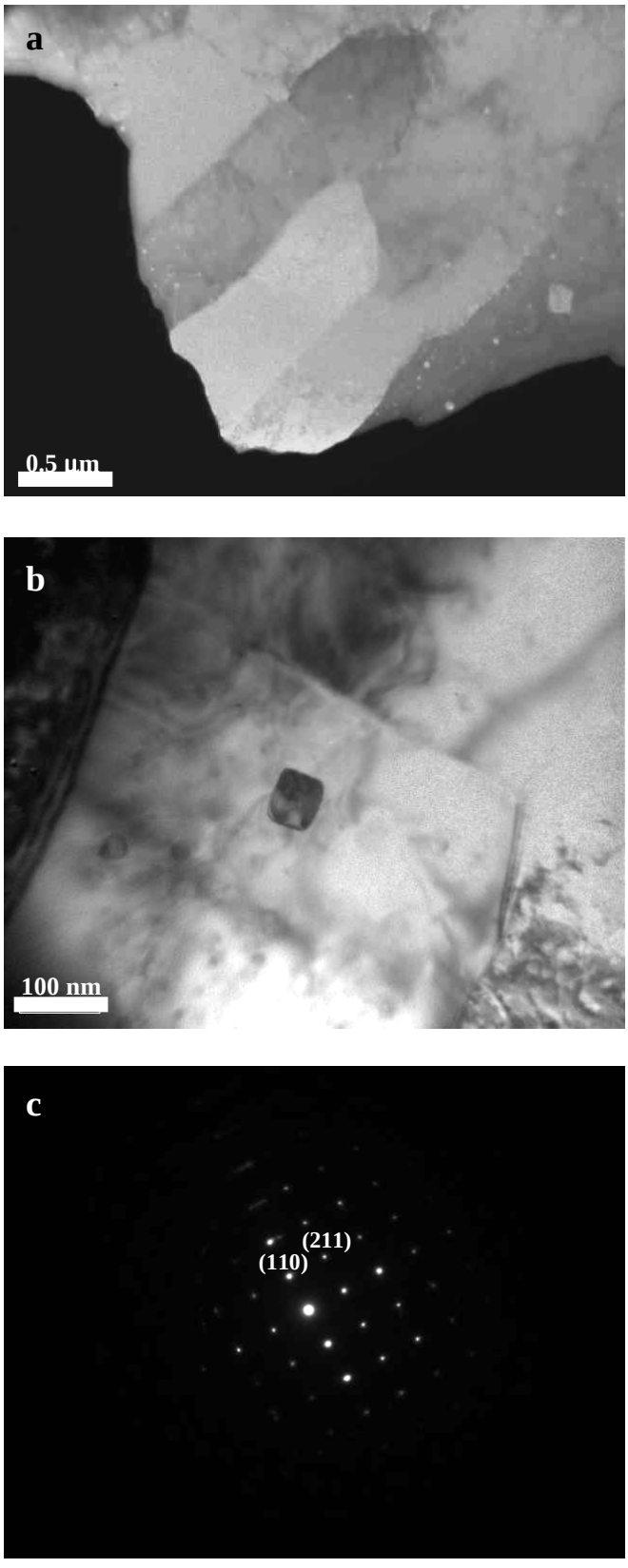

Figure 5.- (a) TEM dark field image of the as-received FeAl Grade 3 intermetallic alloy showing homogeneous grain size and random distribution of some Y_2O_3 particles and (b) SADP of a single grain oriented [$\bar{1}\bar{1}1$].

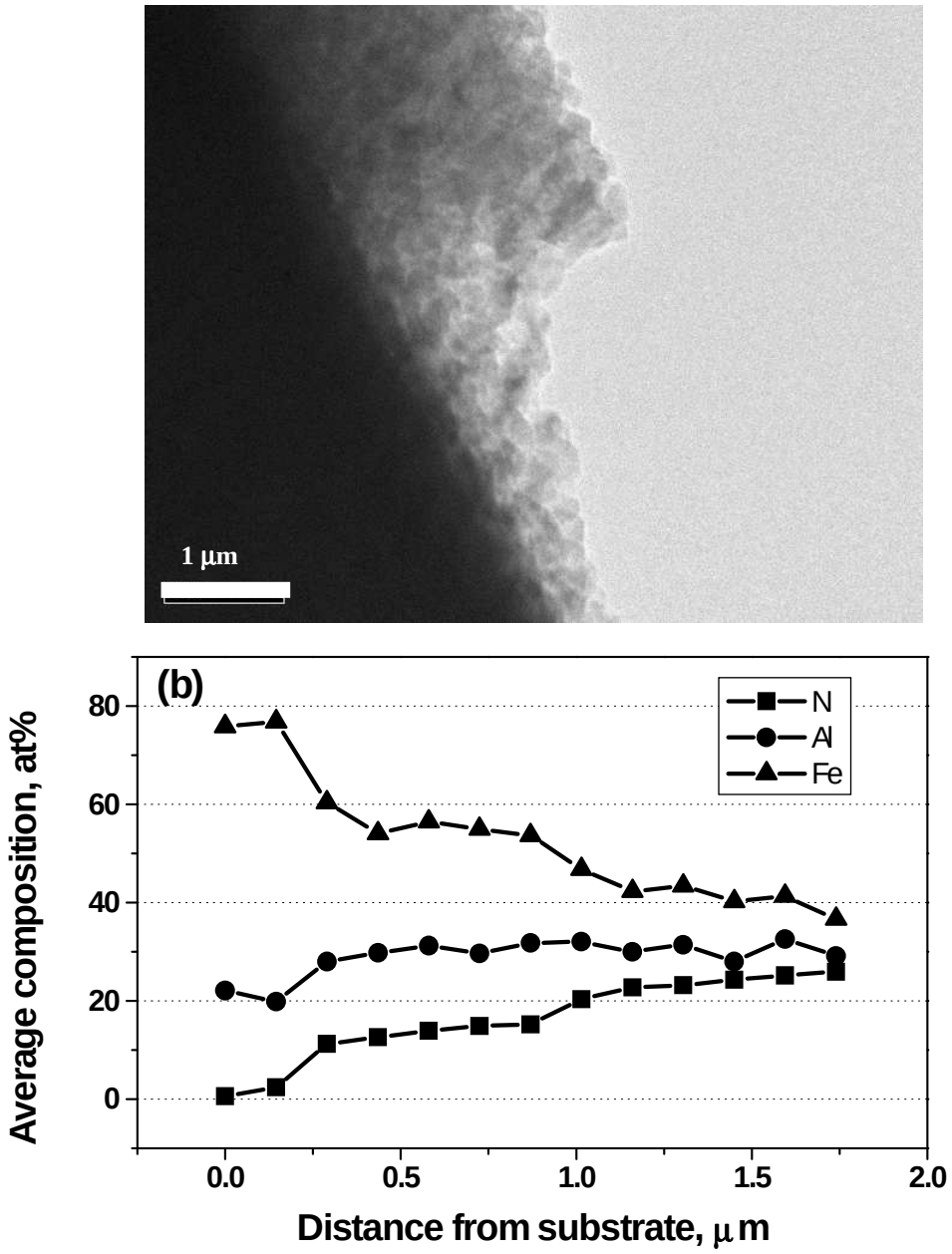

Figure 6.- (a) TEM cross section of the nitrided by implantation-diffusion FeAl Grade 3 substrate showing the nanometer size of this layer and (b) EDS analysis across the nitrided layer.

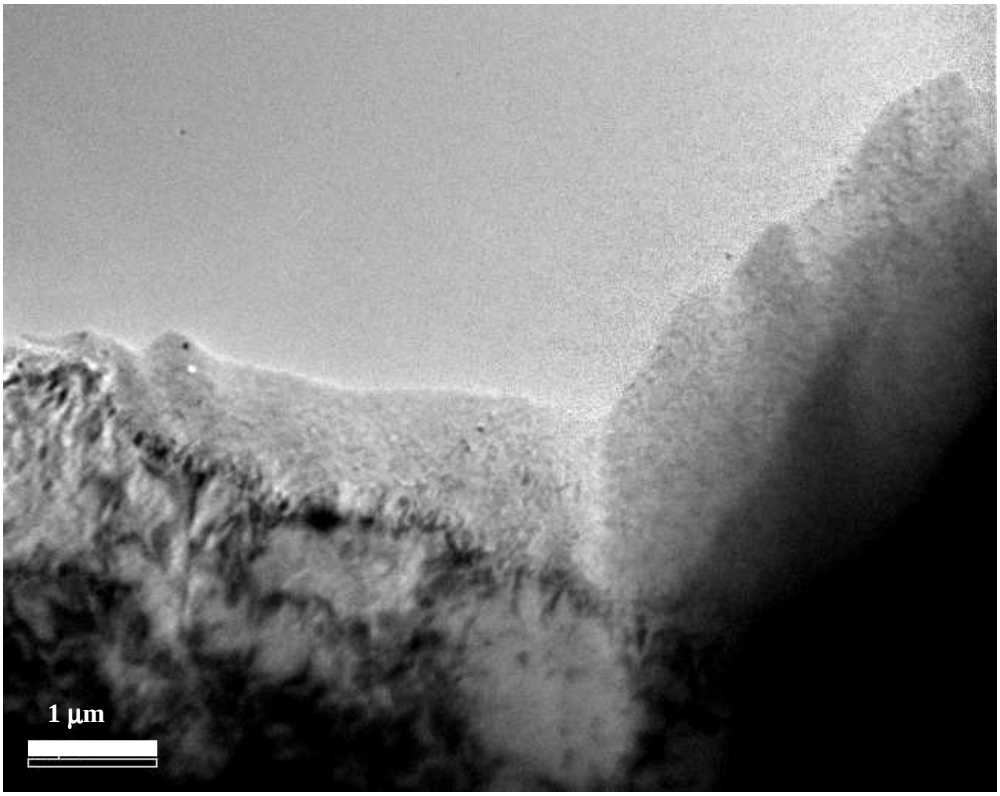

Figure 7.- TEM cross section showing the nitrided layer/substrate interface. The band of α-Fe segregated at this interface between arrows.